On the origin of the long-period tremor recorded at Stromboli volcano (Italy)

Thomas Braun ([1]), **Jürgen Neuberg** ([2]) **and Maurizio Ripepe** ([3])
([1]) *Institut für Geophysik, Stuttgart, Germany*
([2]) *Department of Earth Sciences, Leeds, U.K.*
([3]) *Dipartimento di Scienze della Terra, Firenze, Italy*

Abstract
This investigation deals with the nature of the long-period seismic signals (> 1 s) observed at Stromboli and addresses the question whether they are of volcanic origin or produced by sources such as Ocean Microseisms (OMS). We present results from the analysis of seismic broadband data recorded during 1992 by an array of 9 Guralp CMG-3T seismometers. The determination of the Array Response Function (ARF) shows that array techniques like delay-and-sum beamforming cannot be applied for this purpose, as the extension of the array is limited by the geographical constraint of the island of Stromboli volcano, being simply too small. Spectral analysis reveals three main peaks with periods at 4.8 s, 6 s and 10 s which are not stable in time but vary according to the regional meteorological situation. Whereas 4.8 s and 10 s show up in amplitude spectra calculated during rainy and stormy weather, the 6 s period can be observed during a period of good weather. The signals were first narrowly filtered and then cross correlation, particle motion and amplitudes of the main long periods studied in detail. Relative arrival times as well as seismic amplitudes of the filtered traces do not show any systematic feature but vary with time. Particle motion analysis demonstrates that all long-period signals are recorded by the array as plane waves and that the main propagation direction of the 10 s signal is parallel to the wind direction. No correlation with volcanic activity is obvious. We conclude therefore that the three main long periods are not generated by a close volcanic source. We assume a local cyclone to be the seismic source at 4.8 s and 10 s, which represent the Double Frequency (DF-band) and the Primary Frequency (PF-band), respectively. Concerning the 6 s peak, we speculate a cyclone near the British Isles to act as a seismic source.

Key words *long-period volcanic tremor – ocean microseisms – Stromboli volcano – seismic broadband array*

1. Introduction

It is only a few years that broadband seismometers have been used not only as instruments in observatories, but also for measurements in the field. Instruments used until now are seismometers of type Guralp CMG 3T (Stromboli: Neuberg *et al.*, 1994; Falsaperla *et al.*, 1995) and STS-2 (Sakurajima: Kawakatsu *et al.*, 1992; Stromboli: Dreier *et al.*, 1995) with natural periods of 30 s and 100 s respectively. The extension of the seismometer transfer function down to such low frequencies does not necessarily imply that all the seismic signals recorded by the broadband instrument are generated by the same volcanic source. Especially in the long period range other probable seismic sources such as Ocean Microseisms (OMS), swell and wind have to be considered.

In a pilot study performed in 1991, one STS-2 seismometer was installed on Stromboli (198 in fig. 1) and recorded volcanic tremor

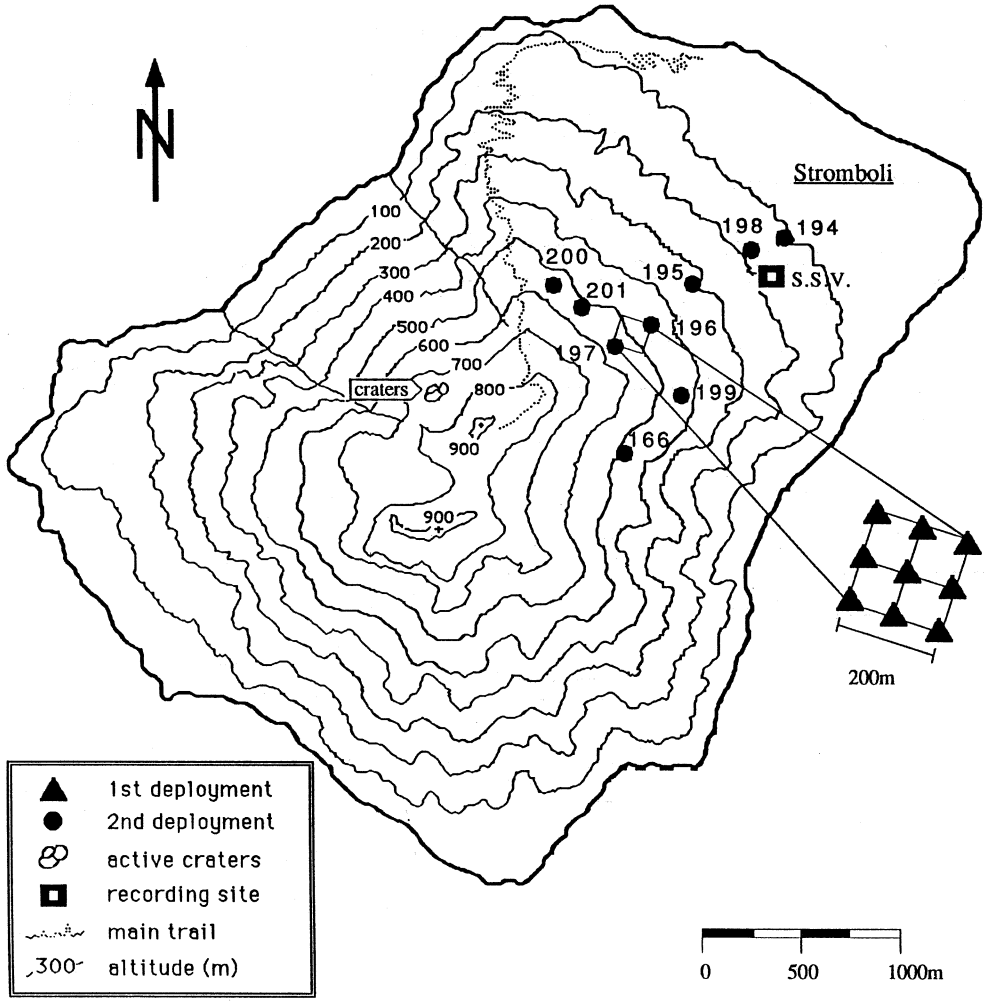

Fig. 1. Sketch map of Stromboli volcano with the configurations of the two seismic broadband arrays. The 1st and 2nd deployment are plotted with triangles and circles respectively.

and explosion-quakes continuously for a period of ten days (Dreier *et al.*, 1995). High spectral energy at periods of about 6 s was reported, but it could not be established whether these low frequencies were generated by a volcanic source or if they were related to OMS or swell. Preliminary results from the analysis of seismic broadband array data recorded at Stromboli one year later, indicated a strong influence of the seismic long periods from wind and ocean induced noise (Neuberg *et al.*, 1994).

In this study we present some considerations on the determination of the propagation direction of the long-period seismic signals. We show a more detailed analysis of the seismic broadband array data recorded in 1992 (Neuberg *et al.*, 1994) and discuss alternative long-period seismic sources.

2. Seismic data

In November 1992 we deployed on Stromboli volcano a seismic broadband array consisting of nine Guralp CMG-3T seismometers with a natural period of 30 s. As shown in fig. 1 the instruments were installed in two different array configurations (1st and 2nd deployment) recording nearly four days each. The first array had a diamond shape with a distance of 100 m between adjacent stations and was designed to investigate the short period wavefield. The aim of the second irregularly spaced array was to study the long periods and azimuthal wavefield distribution. A detailed description of the seismic experiment is given in Neuberg *et al.* (1994).

Analysing the frequency content of the broadband data a considerable part of the seismic energy can be found below 1 Hz (see also Neuberg *et al.*, 1994; Dreier *et al.*, 1995). Figure 2 shows a typical 3-component broadband velocity spectra at station 197 (see fig. 1) calculated for a time interval of 3 h and containing volcanic tremor and explosion-quakes. Long-period spectral peaks (> 1 s) are dominant at 2.3 s, 4.8 s and 6 s.

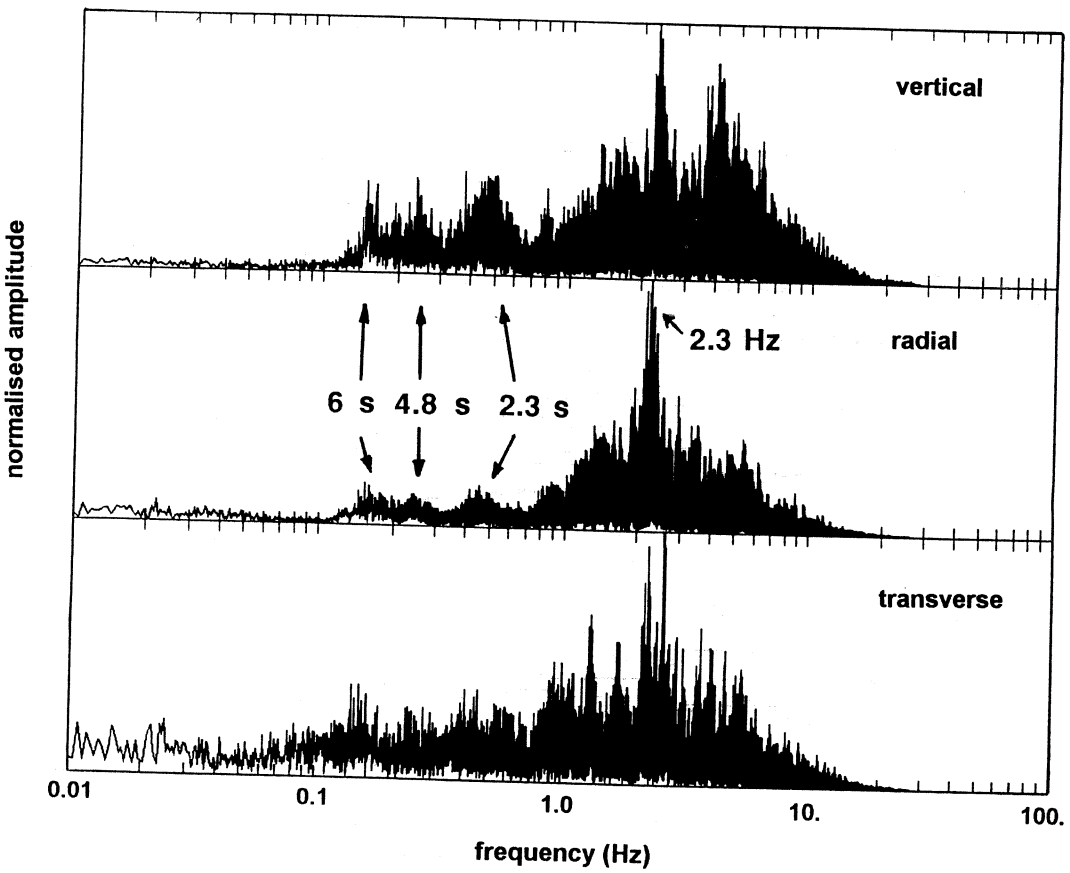

Fig. 2. Typical 3-component broadband velocity spectra recorded at Stromboli volcano (station 197). Note the long-period seismic energy at 2.3 s, 4.8 s, and 6 s.

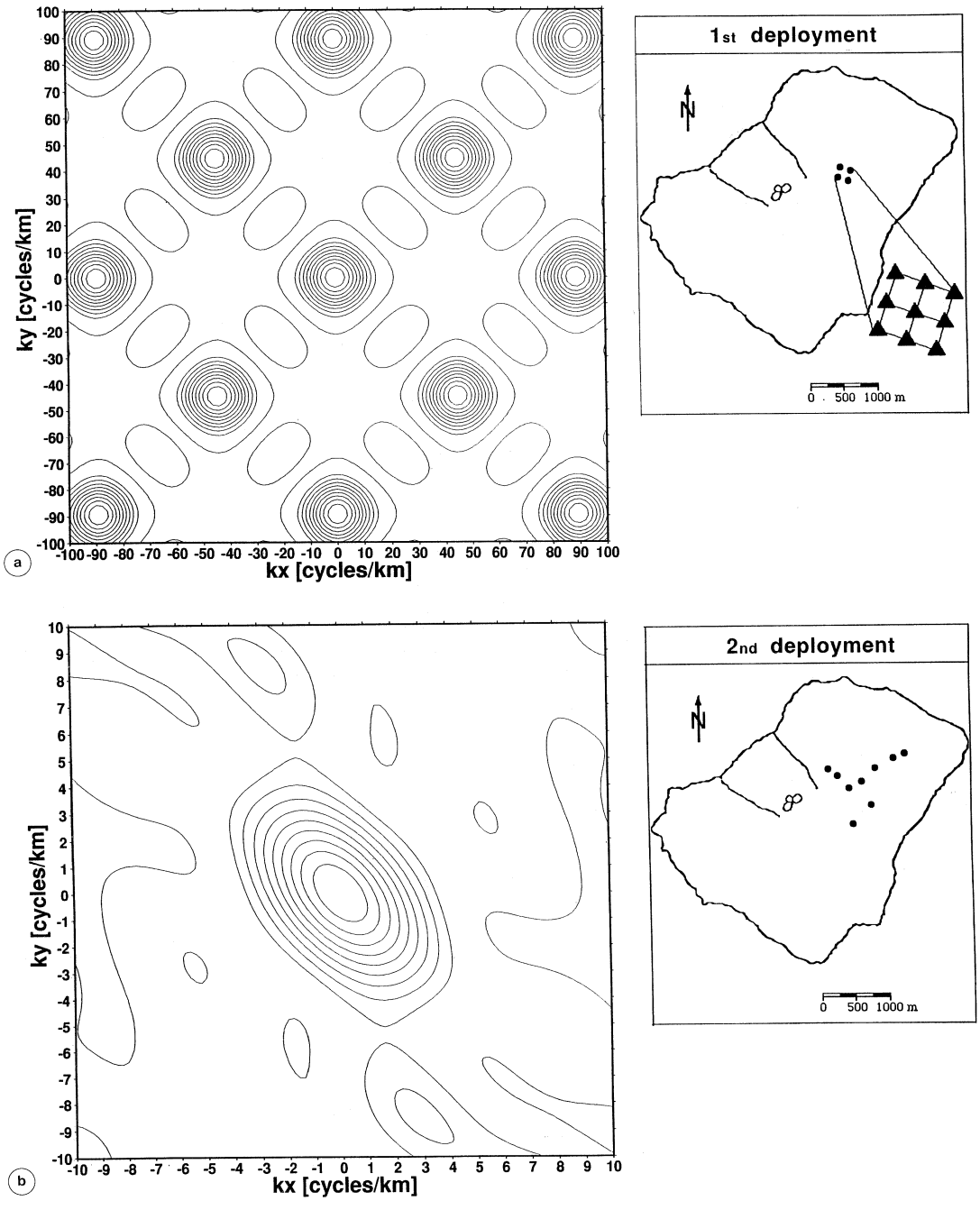

Fig. 3a,b. Array response functions for the 1st deployment (a) and the 2nd deployment (b). On the right side the corresponding station configurations have been plotted in a map.

3. Array characteristics

In order to locate the seismic source(s) of the long-period parts in the volcanic tremor, the wave propagation directions of the dominant frequencies have to be determined. Using data from nine seismic broadband stations this problem could be generally solved applying array techniques like *delay-and-sum beamforming* (see *e.g.*, Harjes and Henger, 1973). This method can be applied only to plane wavefronts, which is the case if either the array dimensions are small or the source is very distant. The seismic arrays deployed on Stromboli volcano had an extension in the range of the distance from the active craters. Therefore the assumption of plane waves is valid only if the long-period tremor is not locally generated by the volcano but belongs to a remote source like swell originated microseisms. In order to calculate the wavenumber range the different arrays can resolve, the receiver characteristics $A(\vec{k})$ of the array have to be studied:

$$A(\vec{k}) = \frac{1}{L} \sum_{n=1}^{L} e^{(-i\vec{k} \cdot \vec{r}_n)}. \qquad (3.1)$$

In eq. (3.1) L is the number of seismic stations and $\vec{k}$ represents the wavenumber vector. $A(\vec{k})$ is also called Array Response Function (ARF) and can be considered as a Fourier transform of the array configuration $\vec{r}_n$. Assuming for the OMS a period of T_{OMS} = 6 s, propagating with a typical apparent wave velocity of c = 2.5 km/s the expected wavenumbers are

$$\vec{k} = \omega \cdot \vec{\alpha} = \frac{2\pi}{T_{OMS} \cdot c} = 0.42 \frac{\text{cycles}}{\text{km}}. \qquad (3.2)$$

In order to check if the array extensions are large enough to resolve these wavenumbers we calculated the ARFs for the arrays deployed at Stromboli in 1992 (fig. 1). Figure 3a shows the ARF for the 1st deployment. With the small dimensions of 200×200 m only wavenumbers of $\vec{k} \geq 22$ cycles/km are resolvable. Figure 3b shows the ARF for the larger 2nd deployment. The mainlobe is not symmetric, and wavenumbers from $\vec{k}$ = 4.5 to 7.3 cycles/km can be resolved, depending on azimuth. Obviously the extension of both arrays is too small to resolve the required wavenumbers of 0.42 cycles/km, mentioned above.

In order to look for a better array configuration resolving the long periods, we calculated the ARFs of hypothetical arrays with larger extension. The design of a more suitable array is limited by some geographical constraints: Stromboli volcano is 3500 m high and only the uppermost 900 m are above sea level. For this reason the largest array that can be installed on Stromboli cannot exceed the aperture of 4 km. Assuming the stations set at the coast line, the wavenumber resolution ranges from $\vec{k}$ = 1.4 to 2.1 cycles/km, depending on azimuth (fig. 4a). Even in this case the maximal possible extension is not large enough to resolve the typical wavenumbers of the OMS.

A seismometer installed on each of the Eolian Islands (fig. 4b) seems to represent a good arrangement for this purpose. The extension of this array would be 80×40 km, corresponding to a wavenumber resolution of $\vec{k}$ = 0.08 cycles/km and 0.16 cycles/km, respectively. Nevertheless, the shortest distances between the islands are between 10 km and 20 km, leading to sidelobes between $\vec{k}$ = 0.62 cycles/km and 0.32 cycles/km. In this case spatial aliasing is produced, and this is why delay-and-sum beamforming cannot be applied succesfully for the localisation of the long-period seismic signals even in this case. We are therefore forced to neglect the array technique approach and to systematically analyse the array data with regard to spectral amplitudes, arrival time differences and particle motion.

4. Spectral amplitude and weather

Before looking for the propagation direction of the long-period parts in the volcano-seismic signals the frequencies of the dominant peaks have to be precisely determined and their stationarity has to be checked. For this purpose

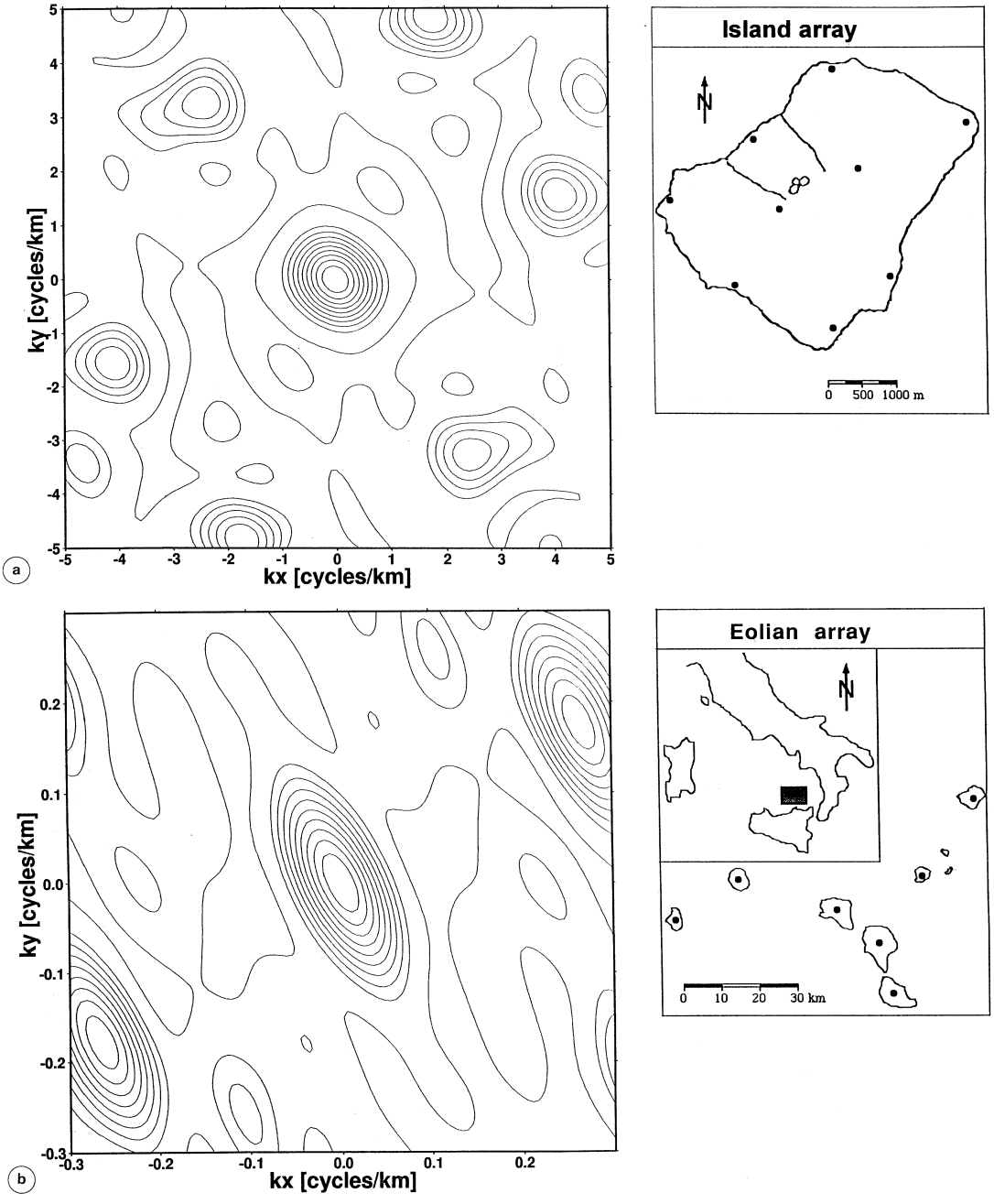

Fig. 4a,b. Array response functions for two hypothetical deployments: a) Island array: seven stations along the coast of Stromboli plus two central stations; b) Eolian array: one station on each of the Eolian islands. The corresponding geographical station positions are plotted on the right side of the figures.

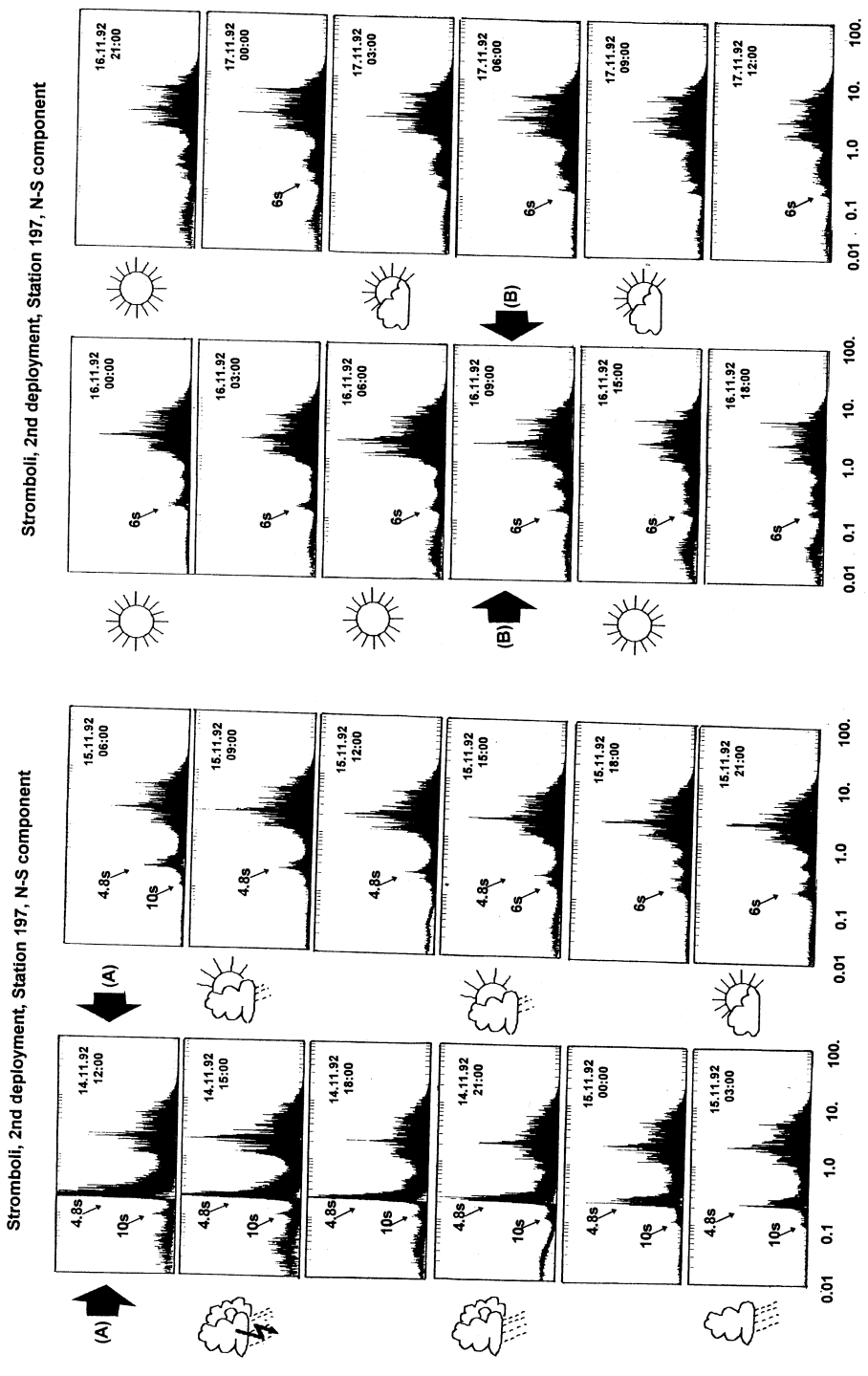

Fig. 5. Temporal variation of amplitude spectra (station 197, N-S component) for a time interval of 75 h. Each of the spectra has been calculated for a 3 h time series consisting of volcanic tremor and explosion-quakes. Note the correlation between spectral amplitude and the meteorological situation plotted with simplified *weather icons*. The arrows indicate the time periods that have been chosen for further investigation.

the continuous time series was plotted for the entire recording period of 75 h (for the 2nd deployment) and the overall spectra of volcanic tremor and explosion-quakes were calculated every three hours. Figure 5 shows the temporal variation of the amplitude spectra recorded by the N-S component of station 197 (fig. 1). The frequency is plotted in logarithmic scale whereas the amplitude of the 24 single figures is plotted in a linear scale normalised to a value of 1600 $\mu m/\sqrt{Hz}$. The single amplitude values can therefore be directly compared. Small icons beside seismic spectra indicate qualitatively the actual weather situation.

The seismic record of the 2nd deployment started on 14th November 1992 during a rainy and stormy period. During 15th November 1992 the weather situation improved, wind calmed down and the day after, sunny weather followed. Figure 5 shows that during the *bad weather* period, high amplitudes at periods between 4.5 s and 5 s could be observed (from now on mentioned as 4.8 s). They decayed according to the weather improvement and disappeared completely in the evening of 15th November 1992. As the same time a smaller peak at about 10 s showed up and can be noted in fig. 5. It occurred only during the highest amplitudes of the 4.8 s and disappeared the morning of 15th November 1992. Nevertheless, following the weather improvement a new spectral peak at 6 s could be observed, starting in the evening hours of 15th November 1992 and remaining stable until the end of the recording period, 17th November 1992.

Even without a more detailed signal analysis the correlation between the main long periods and the meteorological situation is remarkable and suggests that non-volcanic sources make a considerable contribution to the so called long-period volcanic tremor, recorded with broadband seismometers.

5. Data selection

In order to study in more detail the dominant low frequency parts in the volcano-seismic spectra (fig. 5), we selected two typical time windows where they could be clearly identified:

(A) 14.11.1992; 13:25, *bad weather*, for the study of the 10 s / 4.8 s signals,

(B) 16.11.1992; 11:25, *good weather*, for the study of the 6 s signals.

Within these time windows (A) and (B) – indicated by arrows in fig. 5 – we selected a shorter time interval where no volcanic explosion-quake occurred, in order to study signals associated only with *volcanic tremor*. Figure 6a,b shows the selected 6 min and 9 min time intervals respectively for the main *bad* (A) and *good weather* (B) periods from all stations. Traces in fig. 6a,b are unfiltered and plotted in the same linear scale. They are normalised to a maximum value of 50 mm/s. Their amplitudes can therefore be directly compared. Note the low frequency content during the rainy and stormy weather (fig. 6a), comparable to OMS recordings described by many authors (*e.g.*, Strobach, 1964 and 1965). These wavegroups – comparable to the quasi periodic oscillations of beating phenomena – are absent during *good weather* (fig. 6b).

6. Data analysis

6.1. *Filtering*

The two selected *bad* and *good weather* time windows (A and B) were filtered according to the three main periods (4.8 s, 10 s and 6 s) even if they could not be observed in the spectra. This signifies that, *e.g.*, the 10 s signal was analysed in the time window (A) (*bad weather*), as well as in time window (B) (*good weather*). For this purpose we applied a recursive Butterworth Filter (degree 6, forward and backward) with characteristics listed in table I, where T_{center} is the period to be maintained, T_1, T_2 are the low-cut and high-cut periods and f_1, f_2, the corresponding low-cut and high-cut frequencies with the bandwidth *df*.

6.2. *Coherence*

Figure 7a,b shows the seismic traces of fig. 6a,b, filtered around 10 s (table I). The upper plot is from the *bad weather* period (A) and

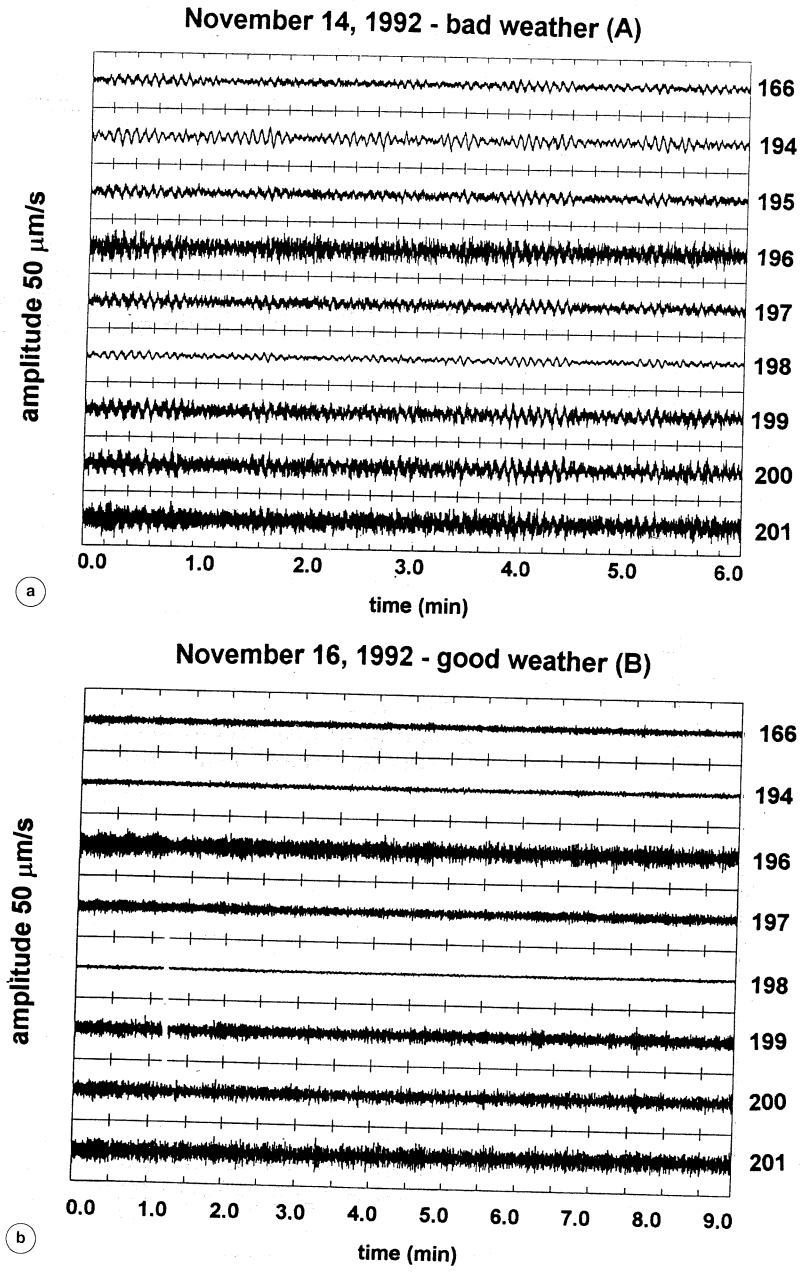

Fig. 6a,b. Unfiltered tremor seismograms (without volcanic explosion quakes) recorded on the radial component of all the array stations during (a) the *bad weather* (A, 14.11.1992) and (b) the *good weather* (B, 16.11.1992) periods (see also corresponding plots n. 1 and n. 16 in fig. 5). Note the long-period wavetrains occurring during the *bad weather* period. The numbers at the right ordinate indicate the respective station number from fig. 1.

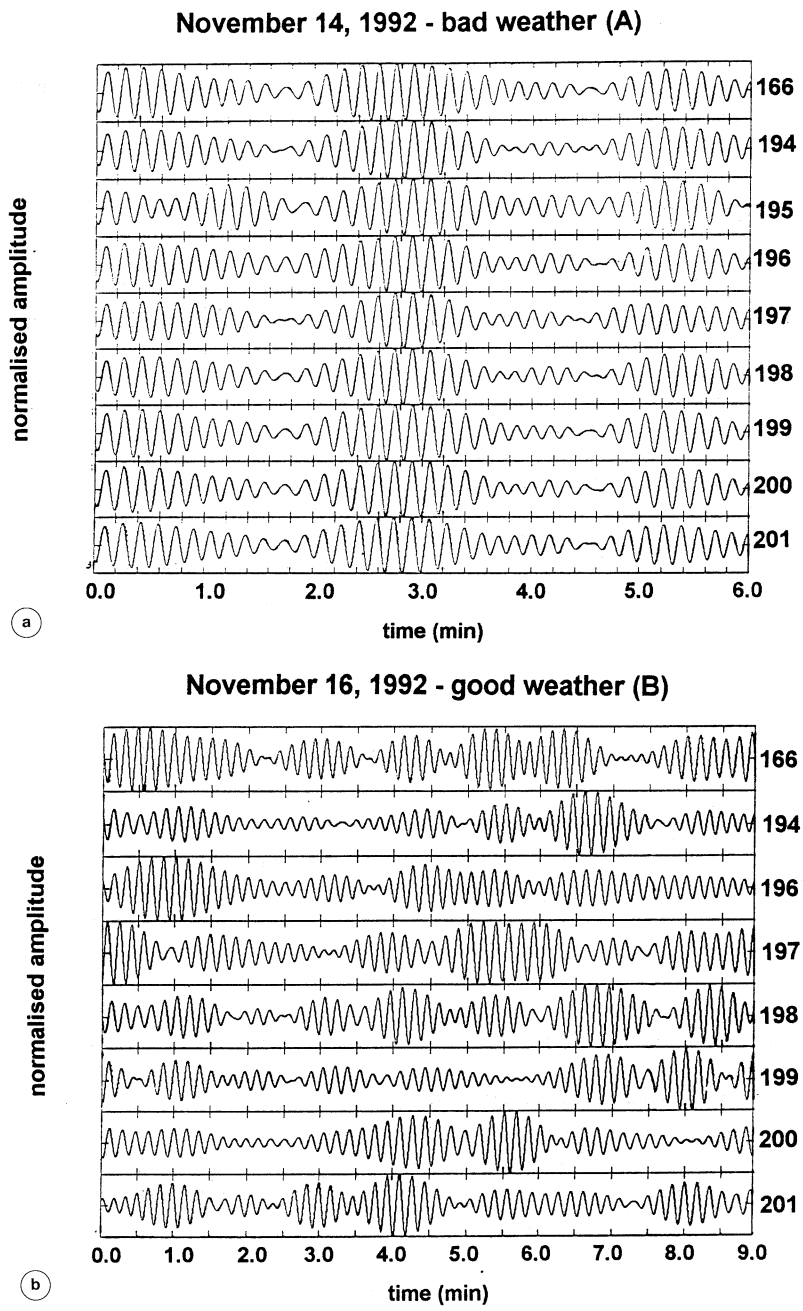

Fig. 7a,b. Seismograms from fig. 6a,b filtered around 0.01 Hz with the Butterworth-bandpass listed in table I. The 10 s signal is coherent over the entire array during (a) the *bad weather* period, whereas during (b) *good weather* no coherence can be observed. The numbers at the right ordinate indicate the respective station number from fig. 1.

Table I. Filter characteristics of the narrow recursive Butterworth filter used to bandpass the broadband seismograms. Listed are the center period (T_{center}), the low-cut and high-cut periods (T_1, T_2) and frequencies (f_1, f_2), the corresponding bandwidth df and the coherence time t_c (eq. 6.1).

T_{center} (s)	T_1 (s)	T_2 (s)	f_1 (Hz)	f_2 (Hz)	df (Hz)	t_c (s)
4.85	5.32	4.39	0.188	0.228	0.04	8
6.50	7.14	5.88	0.140	0.170	0.03	11
10.1	11.11	9.09	0.110	0.090	0.02	16

shows coherent wavefield over the entire array. However, during the *good weather* interval (B) signals at different stations are completely incoherent. This result was partially expected, because the 10 s peak could only be observed in spectra recorded during rainy and stormy weather conditions. This result can be used as a proof that coherence is not artificially caused by digital filtering. We performed the same procedure for the other long periods of 4.8 s and 6 s, obtaining similar results: coherent wavefield could only be observed if identified in the spectra.

6.3. *Cross correlation*

In order to determine the azimuth of the incident wavefront from arrival time we cross-correlated traces among themselves. Despite the high correlation coefficients (> 0.9) no systematics in the arrival times could be found. The arrival time sequences at different stations are not stable varying within short time intervals. Such variation was not to be expected if signals were generated by a local volcanic source.

6.4. *Particle motion*

Applying a narrow filter to a stationary random signal, the particle motion is forced to describe an ellipse, for a time span called coherence time t_c (Seidl and Hellweg, 1991). The coherence time t_c depends on the filter bandwidth df and can be calculated as (Seidl and Hellweg, 1991):

$$t_c = \frac{1}{\pi \cdot df}. \qquad (6.1)$$

If a 3-component seismic trace is filtered with a narrow bandpass of bandwidth df the corresponding particle motion is significant only if it remains stable for a time span as long as the corresponding coherence time t_c. The respective coherence times for the used narrowband filters are listed in table I.

Figure 8a-c shows the horizontal components of the particle motion for the 4.8 s (a), the 10 s (b) and the 6 s (c) plotted for a 6 min duration. The signals were filtered with the narrow bandpass as described in table I. The single plots in fig. 8a-c have been arranged in scale according to the position of the recording station in the 2nd deployment (note the scale and the North direction).

Concerning the *bad weather* recordings (A), we can observe that the particle motion pattern of the 4.8 s signal shows no preferential direction (fig. 8a). Wavefronts arrive from every direction. However, the 10 s signal is mainly longitudinally polarised in the N120°E direction (fig. 8b). Clear and stable longitudinal polarisation can be observed for at least 50 s, a time span three times longer than the coherence time (t_c = 16 s). The result is hence significant and not due to an artificial filter effect.

Concerning the 6 s signal of the *good weather* period (B) the polarisation does not have the clear longitudinal characteristic as for the 10 s signal but a preferential azimuth in the direction of N140°E can be observed (fig. 8c).

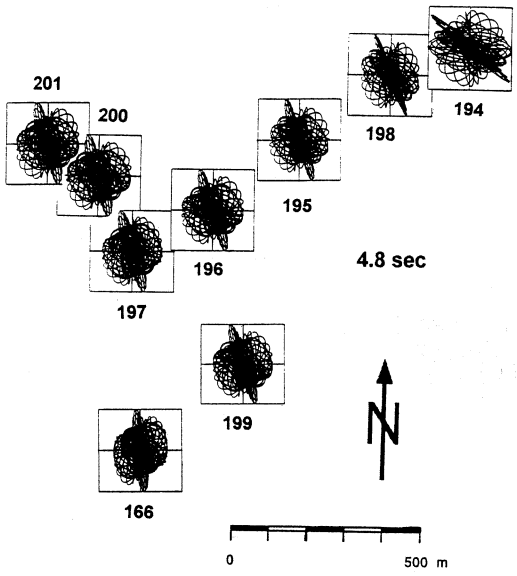

(a) November 14, 1992 - bad weather (A)

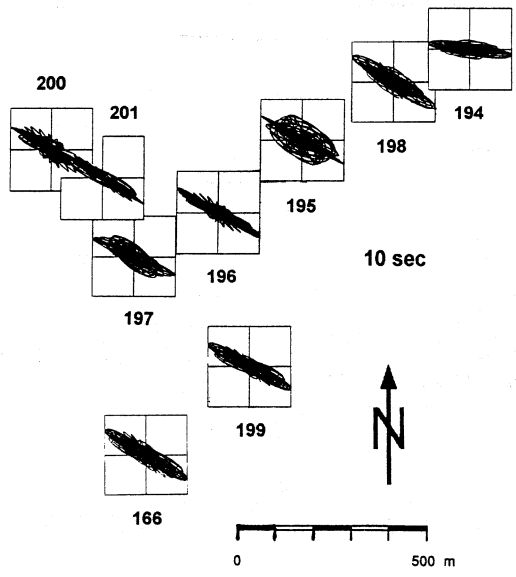

(b) November 14, 1992 - bad weather (A)

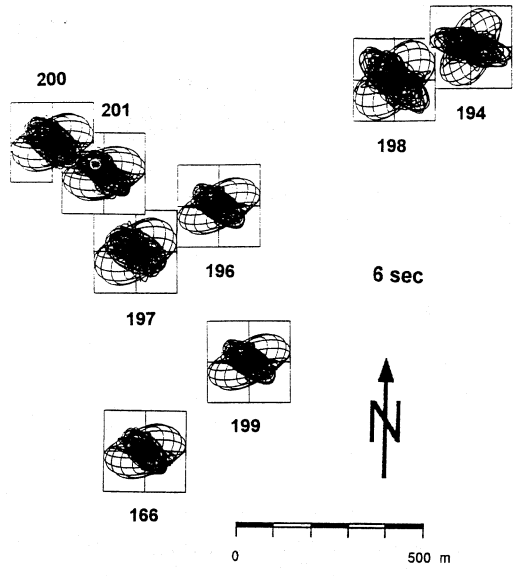

(c) November 16, 1992 - good weather (B)

Fig. 8a-c. Particle motion plots for the narrowly bandpass filtered signals around (a) 4.8 s, (b) 10 s and (c) 6 s. The single plots have been arranged in scale, according to the position of the seismometers station in the 2nd deployment (note the scale and the North direction).

Table II. Spectral amplitude [(mm/s)/Hz$^{1/2}$] and amplitude ratio of the main long periods recorded on the horizontal and vertical component.

Tremor period	Seismic amplitude [(mm/s)/Hz$^{1/2}$]		Ratio
(time window)	horizontal	vertical	horiz./vert.
4.8 s (A)	5000	2000	2.5
10 s (A)	750	45	> 20
6.0 s (B)	450	140	3.2

Each investigated period shows particle motions displaying the same pattern for every array component. An exception to this is station 194 (see fig. 1), where the mean azimuth shows systematically a decrease of 20° if compared to all the other stations. This is probably due to a local magnetic anomaly or to a non correct orientation of the instrument.

Nevertheless, we conclude from particle motion analysis of the filtered traces, that whichever the case, the long periods of 4.8 s, 6 s and 10 s are recorded by the array as plane waves, therefore not being generated by a local and close volcanic source.

6.5. *Amplitudes*

No dependence of amplitude on station altitude could be observed. We therefore assume differences in signal amplitudes at different stations for unfiltered recordings (fig. 6a,b) as due to the site effect. Table II shows the spectral amplitude [(mm/s)/$\sqrt{\text{Hz}}$] of the main long periods, recorded on the horizontal and the vertical components of station 197 (fig. 1).

Signal amplitudes on the horizontal components are always larger than vertical ones for the three main periods. For the 4.8 s and the 6 s the horizontal to vertical component ratio is about 3. Nevertheless, for the 10 s this ratio is much higher (> 20), since here the vertical component never exceeds the noise level.

6.6. *Correlation with volcanic activity*

After the drastic changes of the long-period tremor in frequency, as well as in amplitude, we looked for a correlation with the volcanic activity. Commonly the short period volcanic tremor is understood as representing a volcanic activity parameter (*e.g.*, Schick, 1988), expressed in terms of root mean squared seismic amplitude (rms-value). This criterion is not valid if seismic broadband data are used, because high rms-values (fig. 6a) are produced by a long-period wavefield with no volcanic origin. Besides this, the variation of the rms-value can be estimated from fig. 5. Seismic energy above 1 Hz remains nearly stable during the recording interval of 75 h and weather improvement does not affect the records. Not even the number of explosion-quakes changes, showing a stable value of 11-14 explosion-quakes per hour.

7. Discussion and conclusions

Wavenumber characteristics of different array configurations on and around Stromboli volcano show that typical wavenumber values of 0.42 cycles/km for OMS cannot be resolved with delay-and-sum beamforming.

Detailed analysis of the narrow filtered signal shows that periods of 4.8 s and 10 s appear only during times of *bad weather* (A), whereas the 6 s can be observed only during *good weather* (B). We exclude that the three long periods are produced by a volcanic source such as an oscillating magma chamber beneath the volcano for the following reasons:

– particle motion analysis demonstrates that the array records plane waves (fig. 8a-c) – an indicator for a remote seismic source;

– seismic energy is much higher on horizontal components, which excludes a deep source;

– neither from arrival times, nor from seismic amplitudes can a propagation sequence be determined.

We assume that the three major long-period signals recorded at Stromboli volcano are part of the OMS and are caused by the actual meteorological situation.

Possible sources of the OMS have been widely studied in the past (Darbyshire, 1950; Longuet-Higgins, 1950; Hasselmann, 1963; Haubrich *et al.*, 1963; Strobach, 1965; Gordeev, 1990; among others). It has been observed that the recorded seismic periods are often half the periods of the dominating ocean waves (*e.g.*, Darbyshire, 1950; Haubrich *et al.*, 1963). The observation of the so called Double Frequency (DF-band) is consistent with the theoretical model of Longuet-Higgins (1950), which describes standing waves as an OMS source.

At stations installed near coasts or on islands, additionally weaker amplitudes can be observed within the Primary Frequency (PF-band). These periods have been associated with strong winds (Oliver and Ewing, 1957; Gordeev 1990).

The long-period seismic signals at a frequency twice the PF-band show high energy content and are well known. Haubrich *et al.* (1963) report up to 100 times more seismic energy for the DF-band than for the PF-band.

In our data, the unfiltered seismogram recorded during *bad weather* (fig. 6a) is very similar to the *quasi periodic* oscillations of the OMS, as described, *e.g.*, by Strobach (1964). The typical seismic *bad weather* long periods at 4.8 s and 10 s (A in fig. 5) show the frequency relation 2:1, described, *e.g.*, by Haubrich *et al.* (1963). Seismic energy – roughly estimated from table II as squared amplitude in the horizontal components – shows 50 times higher values for the 4.8 s (DF-band) than for the 10 s (PF-band).

Looking at the particle motion plots (fig. 8a,b) no polarisation can be found for the 4.8 s signal as would be expected from microseisms generated by swell. Nevertheless, the particle motion pattern of the 10 s signal shows a clear longitudinal polarisation in N120°E, which is identical to the wind direction, determined from a meteorological map of November 14, 1992, 12:00 GMT (fig. 9). The lack of energy on the vertical component (see table II) leads us to the conclusion that the 10 s signal is caused by the wind, generating ground inclination, rather than propagating waves. This result is consistent with a study of Berckhemer and Akasche (1966) on seismic ground noise and wind, at the seismological observatory Gräfenberg-Germany (GRF). The amplitudes of the 4.8 s and the 10 s signals decrease in time, following the weather changes as shown in fig. 10, where the meteorological situation in Europe is represented day by day, starting on 14th November 1992. A low pressure area, located on the Thyrrenian Sea 14th November 1992, moved quickly eastward. Wind reached velocities up to 160 km, blowing from WNW (fig. 9).

On the basis that:

i) the actual wind direction was identified in the seismogram (10 s in figs. 8b and 9),

ii) the seismic amplitudes of the *bad weather* periods (4.8 s, 10 s) decreased with weather changes (figs. 5 and 10),

iii) the 4.8 s and 10 s signals show the PF/DF-band characteristics,

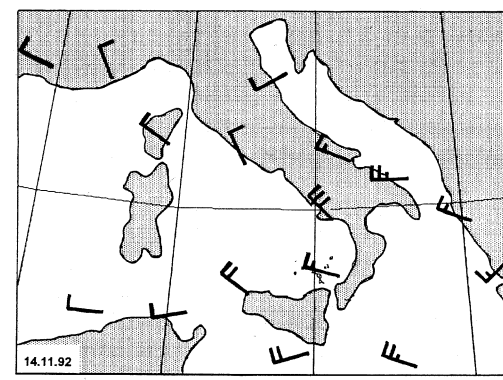

Fig. 9. Wind direction (horizontal line) and wind velocity (vertical line) at November 14, 1992 taken from a meteorological map. One vertical line corresponds to 30 kt per hour.

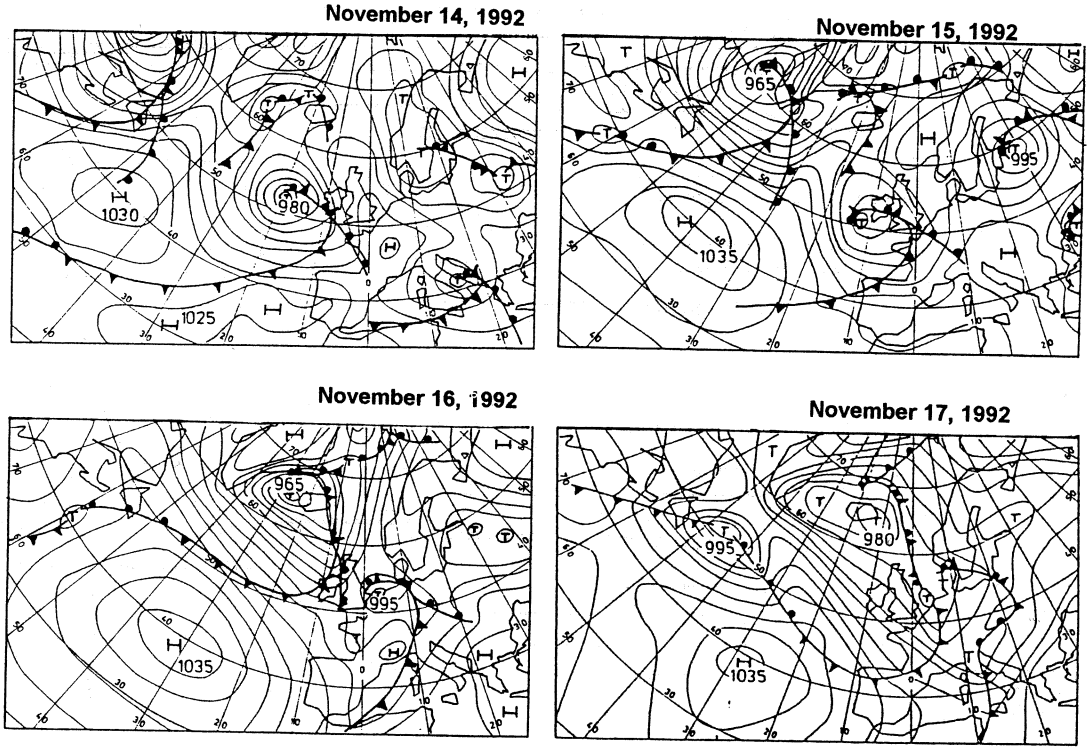

Fig. 10. Development of the meteorological situation in Europe, between 14th and 17th November 1992.

iv) we have not been able to identify any change in volcanic activity,

we conclude that 4.8 s and 10 s periods were generated by the cyclone that passed quickly south of Italy during 14th November 1992 (fig. 10).

As for the 6 s peak the interpretation is more difficult. The propagation direction (N140°E in fig. 8c) we observed is slightly different from that one determined for the 10 s signal, during the *bad weather* interval. Even in this case no indication for a volcanic origin has been found and also the 6 s signal seems to be generated by the OMS. For seismic broadband stations located on the continent, such as GRF (Henkes, 1991), the 6 s period is already known as OMS generated in the Atlantic region. Looking at fig. 10 a strong low-pressure area near England can be localised after 15th November 1992 moving slowly towards Europe. This cyclone could be responsable for the occurrence of the 6 s period in the seismic signal recorded at Stromboli volcano.

Acknowledgements

We are grateful to D. Francis, R. Luckett, T. Pointer, S. Bitossi, L. Gambassi, N. Luise, M. della Schiava for their assistance during the field experiment. We thank H. Dieterich for his suggestions concerning the interpretation of the weather maps. Furthermore we would like to thank E. Gordeev, and R. Schick for critical reading of the manuscript and many helpful discussions. The project has been supported by the Nuffield Foundation, the Leeds University Research Fund, the British Council, and the CNR-GNV.

REFERENCES

BERCKHEMER, H. and B. AKASCHE (1966): Seismic ground noise and wind at the seismological observatory GRF, *Special Scientific Report*, **1**, Univ. Frankfurt, 1-26.

DARBYSHIRE, J. (1950): Identification of microseismic activity with sea waves, *Proc. R. Soc. London, Ser. A.*, **202**, 439-448.

DREIER, R., R. WIDMER, R. SCHICK and W. ZÜRN (1995): Stacking of broadband seismograms at Stromboli *Acta Vulcanol.*, **5**, 165-172.

FALSAPERLA, S., H. LANGER, B. MARTINELLI and R. SCHICK (1995): Seismic measurements on Stromboli volcano in a wide frequency band, *Acta Vulcanol.*, **5** (in press).

GORDEEV, E. (1990): Generation of microseisms in the coastal area, *Phys. Earth Planet. Int.*, **63**, 201-208.

HARJES, H.-P. and M. HENGER (1973): Array-seismologie, *Zeitschr. f. Geophys.*, **39**, 865-905.

HASSELMANN, K. (1963): A statistical analysis of the generation of microseisms, *Rev. Geophys*, **1**, 177-209.

HAUBRICH, R.A., W.H. MUNK and F.E. SNOWGRASS (1963): Comparative spectra of microseisms and swell, *Bull. Seism. Soc. Am.*, **53** (1), 27-37.

HENKES, D. (1991): Arrayuntersuchung des meeresmikroseismischen Wellenfeldes unter besonderer Berücksichtigung seines stochastischen Charakters, *Master Thesis, Univ. Frankfurt*, pp. 96.

KAWAKATSU, H., T. OHMINATO, H. ITO, Y KUWAHARA, T. KATO, K. TSURUGA, S. HONDA and K. YOMOGIDA (1992): Broadband seismic observations at the Sakurajima volcano, Japan, *Geophys. Res. Lett.*, **21**, 1959-1962.

LONGUET-HIGGINS, M.S. (1950): A theory of the origin of microseisms, *Philos. Trans. R. Soc. London, Ser. A.*, **243**, 1-35.

NEUBERG, J., R. LUCKETT, M. RIPEPE and T. BRAUN (1994): Highlights of a seismic broadband array on Stromboli volcano, *Geophys. Res. Lett.*, **21**, 749-752.

OLIVER, J. and M. EWING (1957): Microseisms in the 11 to 18 second period range, *Bull Seism. Soc. Am.*, **47**, 111-127.

SCHICK, R. (1988): Volcanic tremor-source mechanisms and correlation with eruptive activity, *Natural Hazard*, **1**, 125-144.

SEIDL, D. and M. HELLWEG (1991): Volcanic tremor recordings: polarization analysis, in *Volcanic Tremor and Magma flow*, edited by R. SCHICK and R. MUGIONO, 31-47.

STROBACH, K. (1964): Entstehung und Charakter der Mikroseismik als Resultantschwingung zahlreicher seismischer Oszillatoren, *Zeitschr. f. Geophys.*, **30**, 154-177.

STROBACH, K. (1965): Origin and properties of microseisms from the standpoint of oscillator theory, *Bull. Seism. Soc. Am.*, **55** (2), 365-390.